FAR INFRARED PHOTOCONDUCTORS FOR SPACE-BORNE ASTRONOMY: A REVIEW BASED ON THE MIPS 70 μm ARRAY

G. H. Rieke, E. T. Young, MIPS Ge Team*

Steward Observatory, University of Arizona, Tucson, AZ 85721

*) A. Alonso-Herrero, J. Beeman, M. Bradley, J. Cadien, L. Davidson, J. Davis, H. Dole, E. Egami, C. Engelbracht, K. Gordon. E. Haller, G. Heim, T. Horne, D. Kelly, D. Knight, F. Low, K. Misselt, J. Morrison, G. Rivlis, R. Schnurr, J. Stansberry, C. Thompson, G. Winters

ABSTRACT

Far infrared photoconductors have a variety of practical advantages that have led to their being used successfully in the majority of astronomy missions in this spectral range, and to be planned for a number of missions currently under development. The best currently demonstrated performance agrees well with theoretical predictions for these devices, as shown by an analysis of the performance demonstrated by the Ge:Ga 32x32 pixel array developed for SIRTF. This array should operate at the natural background limit set by the environment of the earth in space. Future development can lead to much larger arrays, lower read noise, and modest improvements in quantum efficiency.

1. INTRODUCTION

Most of our knowledge of the universe at far infrared wavelengths has been obtained with photoconductive detectors, particularly as used in IRAS (the Infrared Astronomy Satellite) and ISO (the Infrared Space Observatory) and planned for SIRTF (the Space Infrared Telescope Facility), Herschel, and Astro-F. The widespread use of these devices can be traced to their many advantages, as summarized in Table 1.

Table 1: *Advantages and disadvantages of far infrared photoconductors*

Advantages	**Disadvantages**
• Excellent NEPs • Construction in large filled arrays • Readouts can operate with no ΔT • "High" operating temperatures (~ 2K) • Integrating detector/amplifier leads to simple multiplexinging, low data rates • Large dynamic range (with gain-switching readouts) • Demonstrated solution of systems level issues for space flight	• Calibration issues • Large cosmic ray cross sections • Modest QE (15 - 25%) • G-R noise (√2 penalty in NEP)

The use of far infrared photoconductors for the great majority of space missions for this spectral region indicates that these advantages have overridden the sometimes serious disadvantages also listed in Table 1. The purpose of this review is to examine the performance achieved against the measure of theoretical limits to performance, and to describe the progress made to mitigate the disadvantages.

Contact information for G. Rieke: Email: grieke@as.arizona.edu, phone 520 621 2832

2. SAMPLE APPLICATIONS

2.1 IRAS

The 60 and 100μm bands in IRAS[1] utilized 15 Ge:Ga photoconductors each. The detectors were read out with transimpedance amplifiers (TIAs) that used JFET first stages that were mounted in a way that isolated them thermally so they could be heated to operate in a low noise and stable regime [2,3]. The TIAs were an optimum choice given the requirement for good frequency response to match the continuous scan of the IRAS survey, and the desire to stabilize the detector biases to improve dynamic range and avoid a number of non-ideal effects. Detector calibration was maintained by flashing reverse bolometer stimulators mounted in the center of the telescope secondary mirror. Cosmic ray effects were erased by boosting the detector bias to breakdown [4]. The intrinsic performance of the detectors was limited by the Johnson noise of the TIA feedback resistors and by other noise sources associated with the readout. The in-flight performance was similar to expectations from pre-flight calibrations.

2.2 ISOPHOT

The ISOPHOT instrument[5] carried a 3x3 array of unstressed Ge:Ga detectors and a 2x2 array of stressed devices. The readout was by a capacitive transimpedance MOSFET amplifier whose processing had been adjusted to improve its performance at low temperatures[6]. The readouts were mounted close to the focal plane and cooled to a similar temperature. Calibration was assisted with a calibration stimulator built into the instrument, and which could be viewed by adjusting the position of a scan mirror. In practice, the unstressed focal plane never achieved the performance level anticipated from laboratory measurements of its NEP. Its observed performance was limited by long time constant behavior associated with residual instabilities in the readouts, with the relatively high operating temperature of the detectors and resulting variable dark current, from the effects of cosmic ray hits, and from the intrinsic slow response of the detectors. The performance of the stressed devices was substantially better, due in part to the relatively large fast response component of these devices (compared with the slow component) and their better thermal isolation from the readout amplifiers.

2.3 Long Wavelength Spectrometer LWS

The LWS instrument on ISO[7] used a single Ge:Be detector, five Ge:Ga devices, and four stressed Ge:Ga detectors. The readouts were based on JFETs, mounted with thermal isolation and heated to a temperature where they operated with good stability and low noise. The readout circuit was an integrating source follower. NEPs of ~ 1 x 10^{-18} W/$Hz^{1/2}$ were measured in the laboratory[8]. Calibration was assisted with built in stimulators that were flashed between spectral scans. On orbit, it was found that frequent small glitches, probably associated with cosmic ray hits, limited the maximum integration times to shorter values than had been anticipated but otherwise the detectors operated approximately as expected from pre-flight calibrations[9].

3. DESIGN FUNDAMENTALS

As summarized above, there is an extensive and generally successful history of use of Ge:Ga photoconductors in space far infrared astronomy. Other papers at this conference will discuss the development of focal planes for Herschel and Astro-F based on these devices. In this section, I discuss the fundamental performance limits for far infrared photoconductor arrays, and illustrate them with the pre-flight measurements of the behavior of the 70μm array developed for SIRTF[10].

3.1 Material Properties

A variety of shallow dopants in germanium could in principle be used for far infrared detectors with photoconductive cutoff wavelengths near 100μm[11]: As (λ_c = 98μm); P (λ_c = 103μm); In (λ_c = 111μm); Ga (λ_c = 115μm); B (λ_c = 119μm); and Sb (λ_c = 129μm). These materials have similar absorption cross sections, σ_i = 1 to 1.6 X 10^{-14} cm^2 [12]. From the barrier height associated with detection at 100μm, a simple quantum mechanical calculation demonstrates that impurity concentrations of ~ 1 x 10^{15} cm^{-3} or more will

lead to large dark currents due to hopping, so high performance material is limited to concentrations of a few times 10^{14} cm^{-3}. Thus, given the fundamental upper limit on dopant concentration and the similarity of ionization cross sections, there is no obvious advantage of one material over another. Ge:Ga is the most mature technology and has been widely employed in focal planes on space-borne telescopes. There is also interest in Ge:Sb because of its longer cutoff wavelength.

3.2 Detector Geometry

The absorption cross sections and maximum impurity concentrations discussed in the preceding section set the basic boundary conditions for detector geometry, since they yield absorption lengths of 1 – 3 cm. A number of considerations lead to a need for detector dimensions substantially less than these absorption lengths – among them are the cosmic ray hit rate in space, and the need to control optical cross talk in detector arrays. The implications of this long absorption length are illustrated by the design of the MIPS array.

The array is based on bars of Ge:Ga that are 4mm long along the direction of photon incidence (see Figure 1). At the back of each bar but not in contact with it is a mirror of aluminized sapphire that reflects escaping photons back into the detector. This geometry provides a total path length of 8mm (ignoring additional reflections from the detector front face and the extra path for photons at off-normal incident angles). Each bar is 32 pixels long into the page as drawn in Figure 1, and the individual pixels are delineated by individual contact pads on the output side of the detectors. Structure to hold the detector bars is hidden by optical concentrators, in the form of optical wedges of intrinsic germanium that are glued to the detector faces.

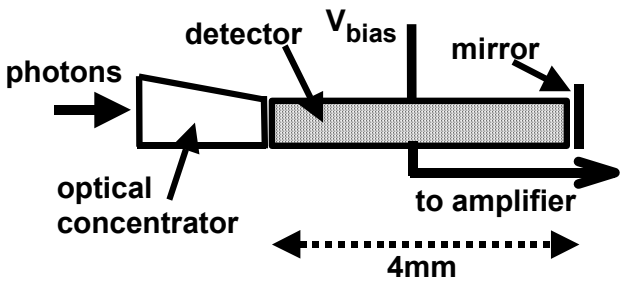

Figure 1 *MIPS Array Detector Geometry*

This design appears to produce the expected absorption efficiency. The Ga concentration in the detector material is 2 x 10^{14} cm^{-3}, and the absorption cross section is 1 x 10^{-14} cm^2, so the absorption length is expected to be 2 cm. The reflection loss at the entry face of the concentrator is 0.36, and at the interface between concentrator and detector is about 0.15. The predicted absorption is therefore $(1 - r_{con}) \times (1 - r_{con/det}) \times (1 - e^{-0.8cm/2cm}) = 0.18$ (ignoring small corrections such as the return reflection from the detector front face). The measured detective quantum efficiency of the detectors is 18%, in fortuitously good agreement with the predicted absorption.

The long absorption path provided by this detector geometry dictates the use of transverse contacts. If a transparent contact geometry were to be used, with a contact spacing of 4mm, the responsivity would be S < 1.5A/W at the primary operating wavelength of 70μm, assuming photoconductive gain G < 1. To reach the photon background limit would require an amplifier with read noise less than 50 electrons rms, which is not currently realizable given the other constraints on the readout such as operating temperature and capacitance in the detector/readout interconnect. The transverse contacts are placed across the 0.5mm thickness of the detector bars, and at a nominal operating bias of 50mV the device provides S = 7 A/W at 70μm. By combining this result with the measured detective quantum efficiency, we derive that G = 0.7.

A final constraint on the detector size is set by optical cross talk requirements, at least in the MIPS arrays where adjacent pixels are all in a single detector bar and are delineated by the contacts. A simple geometric calculation leads to the estimate that, for a projected pixel of $\lambda/2D$ at $\lambda = 100\mu m$ and a pixel length of 8mm, a pixel width of 0.5mm or greater is required for crosstalk less than 2.5%, independent of the telescope aperture. A somewhat larger width of 0.75mm was selected for the MIPS array, both to make construction easier and to allow multiple instrument modes that illuminate the array from slightly different angles. The

most sensitive test of the cross talk is a comparison of the imaging determined in the instrument as it was aligned with optical light, viewed heavily oversampled with a TV camera, and in the far infrared illuminated with pinhole sources at the instrument focal plane. There is no measurable deviation in the far infrared imaging from the predictions of the optical alignment testing. This result shows that the cross talk is < 5%, consistent with expectations.

4. CALIBRATION

At high backgrounds such as might be encountered in an airborne instrument, photoconductors behave relatively well, with rapid adjustment of the detector resistance to a new value appropriate to a new illumination level. As the background is decreased, the adjustment to equilibrium levels occurs in a multiple step process with multiple associated time constants. Thus, the detectors can be used in a straightforward manner at high backgrounds but precautions must be taken at low ones to track the calibration.

4.1 Causes of Calibration Variability

A fast response component results from the current conducted within the detector volume resulting from the drift of charge carriers freed by absorption of photons. The speed of this component is controlled by the recombination time in the material, and hence is in fact very fast by normal detection standards. However, as charge moves within the detector, the electrical equilibrium must be maintained. For example, charge carriers generated by photoionization are removed from the detector when they drift to a contact. They are replaced by injection of new charge carriers from the opposite contact, but the necessity for new charge can only be conveyed across the detector at the "dielectric relaxation time", basically its capacitive or *RC* time constant:

$$\tau_d = \frac{\kappa_0 \varepsilon_0}{\mu\, n_0 q}.$$

Here, κ_0 is the dielectric constant of the material and μ is the mobility for the charge carrier of interest, ε_0 is the permittivity of free space, n_0 is the density of free carriers, and q is the charge on the electron. The form of this time constant makes explicit the dependence on illumination level through the density of free charge carriers, n_o. In fully illuminated detectors (for example, in integrating cavities) and at the low backgrounds appropriate for space-borne operation, τ_d can be tens of seconds.

In transverse contact detectors, the part of the detector volume near the injecting contact may be poorly illuminated and have large resistance. The detector therefore adjusts to a new equilibrium only at the large dielectric time constant of this layer, which can be hundreds of seconds at low backgrounds. The initial shift of charge in the detector can set up a space charge that reduces the field in the bulk of the device, leading to a reduction of responsivity following the initial fast response. From its appearance on a plot of response versus time, this behavior is described as "hook" response. As the field is restored at a characteristic rate of τ_d, the response grows slowly to a new equilibrium value (see Haegel et al.[13] for detailed modeling).

Ionizing particles such as cosmic rays also affect the calibration of these detectors. In a p-type detector such as Ge:Ga, the electrons freed by a cosmic ray hit can be captured by ionized minority impurities, reducing the compensation and increasing the responsivity. A similar process operates in n-type detector material. The shifts in detector characteristics can be removed by warming it to a temperature that re-establishes thermal equilibrium, and then cooling it back to proper operating conditions. Other processes can be partially effective in restoring the behavior, depending on the detector material and the characteristics of its readout.

4.2 Dealing with the Problems

All successful uses of far infrared photoconductors at low backgrounds have included local relative calibrators of reverse bolometer design that allow an accurately repeatable amount of light to be put on the detector. In general, this strategy is most successful when the conditions of measurement are changed the least to carry out the relative calibration.

The MIPS instrument includes such calibrators, and the baseline plan is to flash them every two minutes. Based upon data obtained at a proton accelerator, we expect that the average increase in response over a two minutes period in the space environment will be about 0.5%, so the calibration interval allows tracking the response accurately. An additional precaution to improve the photometric behavior is to take the data in a way that depends primarily on the "fast" detector response. This response should be free of many of the long-term effects that can complicate calibration. To place the signals in the fast response frequency regime, the instrument uses a scan mirror based on the one developed for the SWS instrument on ISO (plans for which were provided by T. DeGraauw) to modulate the signals on the array. Additional important features are that the detectors are operated at about 1.5K, well below the temperature where dark current variability is an issue (at ~ 2.5K and warmer), that the readouts have excellent stability even at their operating temperature of ~ 1.5K[14], and that the heat from the readouts is carefully isolated from the detectors. Finally, the instrument operations force observers to combine many short observations of a source into a single measurement. The high level of redundancy in the data will help identify outlier signals and will also improve the calibration by simple averaging over variations.

These measures appear to be effective in tracking the calibration accurately. For example, Figure 2 shows the accuracy with which a stimulator flash is tracked by the average of the flashes before and after. The standard deviation of the variations is less than 1%, and it includes a significant contribution by shot noise from the stimulator outputs - that is, the detector behavior is tracked to well under 1%. A model calculation by Haegel and Smylie (private communication) shows that the effect of the stimulator flashes on the measured signal from a faint source is small, of order 10% or less. This effect decays rapidly with time after the stimulator flash. The design of the MIPS instrument enforces that observations of a source are made repeatedly and over the full range of times from one stimulator flash to the next, so a simple average of these measurements will return a calibrated measurement to an accuracy of 3 - 4%.

A final issue in utilizing these instrument features is that the instrument must operate efficiently in the cosmic ray environment - if there is a high rate of lost integrations, the redundancy of the observations will be reduced. In practice, lost integration time due to hits is small because the CTIA readout amplifiers maintain detector bias accurately and the data are obtained by sampling up the integration ramp and sending all the samples to the ground. As a result, the integration ramp after a hit can be recovered and used to extend the integration.

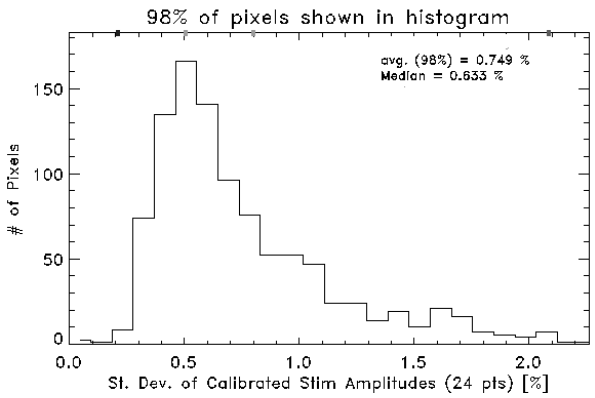

Figure 2 *Result of calibrating stimulator flashes against each other*

Figure 3 illustrates a cosmic ray hit that occurred during instrument tests. A linear least squares fit has been made to the two integration ramps, one before and the other after the hit (with a small number of points immediately after the hit excluded). Figure 4 shows a comparison of slopes before and after similar cosmic ray hits. A large number of hits have been combined and the results are plotted as a function of the size of the jump in the integration ramps. The error bars indicate one standard deviation in the ratio of average integration ramp slopes before and after the hits. There is a very slight tendency for the slope to increase after very large hits, but in general the change in slope is within the read noise and hence data post-hit can be combined with data pre-hit with only a small loss in effective integration time or shift in the calibration.

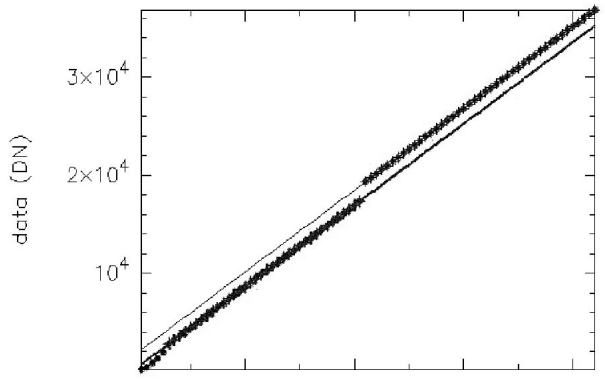

Figure 3 *Cosmic ray hit during instrument test causes a jump in the integration ramp. Slopes have been determined for each ramp segment by fitting lines by least squares. The duration of the integration is about 10.5 seconds and a DN is about 7 electrons.*

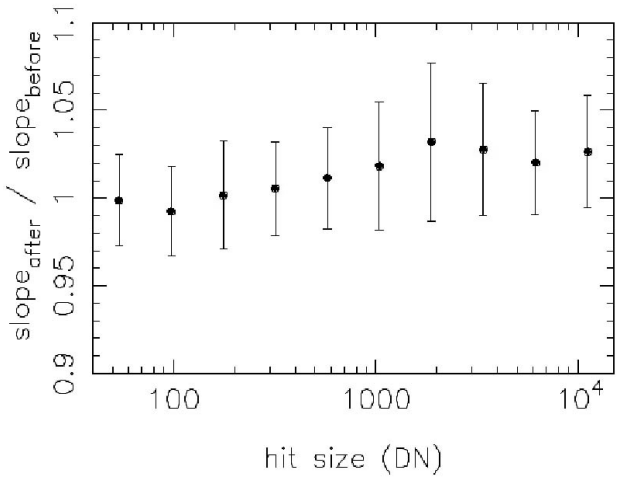

Figure 4 *Comparison of integration ramp slopes before and after a hit and as a function of the size of the hit*

5. ACHIEVED PERFORMANCE

Because the MIPS array design is driven by theoretical limits for the operation of Ge:Ga photoconductors, its performance is of interest as a benchmark for far infrared arrays in general. Table 2 lists some of its salient characteristics.

The cryogenic readouts are critical for obtaining the performance quoted. Two important aspects are the excellent stability at a temperature of ~ 2K (and even below 1K from additional measurements), and the ability of the CTIA circuit to maintain the detector bias during cosmic ray hits and other large signal events. The shortcomings of photoconductors with regard to accurate calibration appear to be manageable with frequent relative response measurements using stimulators in the instrument.

Improvements can be anticipated in a number of areas. The read noise is in agreement with the measured read noise for the bare readouts, degraded by the capacitance of the detectors and the interconnect between them and the readout. Improvements are possible in the readout processing for low noise, and there is a tradeoff in detector size and interconnect capacitance that could be adjusted to achieve lower noise. The detective quantum efficiency could be improved to ~ 25% by applying antireflection coatings to the input face and to the interface between concentrator and infrared-active material. The dynamic range could be improved by using a readout with gain switching. Finally, it is possible to increase the array format, either

by stacking more modules similar to those used in the MIPS array to achieve 32xN pixels, or to expand the format to 64 pixels or more. We are far from fundamental obstacles to any of these improvements. Given the systems level advantages of photoconductors for large arrays, the enhanced performance that is possible will continue to make such devices highly desirable for future infrared astronomy missions.

Table 2 *Performance achieved with MIPS 70μm array*

Parameter	Achieved Value
Format	32x32 pixels, each 750μm square
Operability	99.8% for the flight array
Fill factor	~ 100%
Read Noise	~ 130 electrons rms
Responsivity	7 A/W at 70μm
Detective quantum efficiency	18%
NEP	1 x 10^{-18} W/$Hz^{1/2}$ in 10 s integrations @ 100μm
Calibration Repeatability	Better than 1%
Operating temperature	~ 2K
Dynamic Range	100:1 above "dark" sky

REFERENCES

1. Neugebauer, G., et al. 1984, ApJL, 278, 1
2. Rieke, G. H., Montgomery, E. F., Lebofsky, M. J., and Eisenhardt, P. R. 1981, Appl. Opt, 20, 814
3. Low, F. J., Beichman, C. A., Gillett, F. C., Houck, J. R., Neygebauer, G., Langford, D. E., Walker, R., G., and White, R. H. 1984, AptEng, 23, 122
4. Beichman, C. A., et al. 1988, IRAS Explanatory Supplement, 2nd Edition.
5. Lemke, D., et al. 1996, A&A, 315L, 64
6. Dierckx, B., Vermeiren, J., Cos, S., Faymonville, R., and Lemke, D. 1992, Proc. ESA Symposium on Photon Detectors for Space Astronomy (SEE N94-15025), pp 405 – 408
7. Swinyard, B. M. et al. 1996, A&A, 315L, 43
8. Church, S. E., Griffin, M. J., Price, M. C., Ade, P. A., Emergy, R. J., and Swinyard, B. M. 1993, Proc. SPIE, 1946, 116
9. Burgdorf, M. J., et al. (1998), Adv. In Space Research, 21, 5
10. Young, E. T. et al. 1998, Proc. SPIE, 3354, 57
11. Bratt, P. R. 1977, in Semiconductors and Semimetals, eds. R. K. Willardson and A. C. Beer, 12, 39
12. Wang, J.-Q., Richards, P. L., Beeman, J. W., Haegel, N. M., and Haller, E. E. 1986, Appl. Opt., 25, 4127
13. Haegel, N. M., Schwartz, W. R., Zinter, J., White, A. M., and Beeman, J. W. 2001, Appl. Opt., 40, 5748
14. Young, E. T. 1994, Proc. SPIE, 2226, 21